Dalton Transactions

PAPER

View Article Online
View Journal | View Issue

Cite this: *Dalton Trans.*, 2025, **54**, 16461

Imidazo[1,5]carbachlorin as a hybrid ligand

Kinga Szydełko, Sebastian Koniarz, Michał J. Białek and Piotr J. Chmielewski *

Received 30th October 2024,
Accepted 7th October 2025

DOI: 10.1039/d4dt03034f

rsc.li/dalton

A family of novel complexes of imidazo[1,5]carbachlorin has been synthesized and characterized by spectroscopic, X-ray diffraction, and electrochemical methods. In most of these compounds, both the macrocyclic crevice and the fused external imidazole are involved in the coordination of the metal ion, thus defining imidazocarbachlorin as a hybrid ligand system consisting of NNNC- and N-donor sets. The effect of the external coordination on the shape of the macrocyclic ring has been studied and discussed.

Introduction

N-confused porphyrin (**NCP**), *i.e.*, 2-aza-21-carbaporphyrin (Fig. 1), is an aromatic tetrapyrrole of distinct coordinating properties related to the structural features of the macrocyclic ring.[1–3] Apart from the internal NNNC core that may adopt several coordination modes and geometries and stabilize uncommon oxidation states,[4–31] there is an external nitrogenous donor site located on the peripheries of the macrocycle. Several monomeric and oligomeric transition metal complexes of **NCP** and its derivatives have been reported, where the macrocyclic core and monodentate external N-donor of the *confused* pyrrole are both involved in coordination.[11,14,18,20,32–38] In several of such complexes, ligation of the external nitrogen N2 is supported by *ortho*-metalation of an aryl located at the adjacent *meso*-position C20,[12,38–41] which is accompanied in some instances with a severe distortion of the porphyrinoid geometry. Obviously, such an external ligation of the regular porphyrin **Por** (Fig. 1) requires an additional donor atom or donor set localized at the macrocyclic perimeter, which is well-exposed and points towards the potential coordination center. In this regard, the most interesting seem to be imidazole-fused porphyrins,[42–52] which can also be converted from a potentially N-donating species into the N-heterocyclic carbene ligand (NHC) by alkylation of both imidazole nitrogens.[44–50,53] Owing to the [2,3] *ortho*-fusion mode of the imidazole-pyrrole moiety and the steric factors imposed by the aryls at the *meso*-positions C5 and C20, these derivatives appear to be effective NHC ligands rather than N-donors. In fact, to date, there has been no report regarding N-coordination of porphyrin-fused imidazole. Conversely, in the readily obtainable imidazo[1,5]carbachlorin (**ICC**),[54] the well-exposed nitrogen of the *ortho*-fused imidazole constitutes a promising donor site. However, also for this system, only NHC-type gold(I) extraannular coordination of the *N*-methylated derivative of silver(III) complex of **ICC** (Ag**ICCMe**) has been reported until now (Fig. 1). We thus decided to explore the coordination of the external nitrogen of the **ICC** free base as well as of its complexes with inert d^8 transition metals, as well as boron(III). Special attention will be

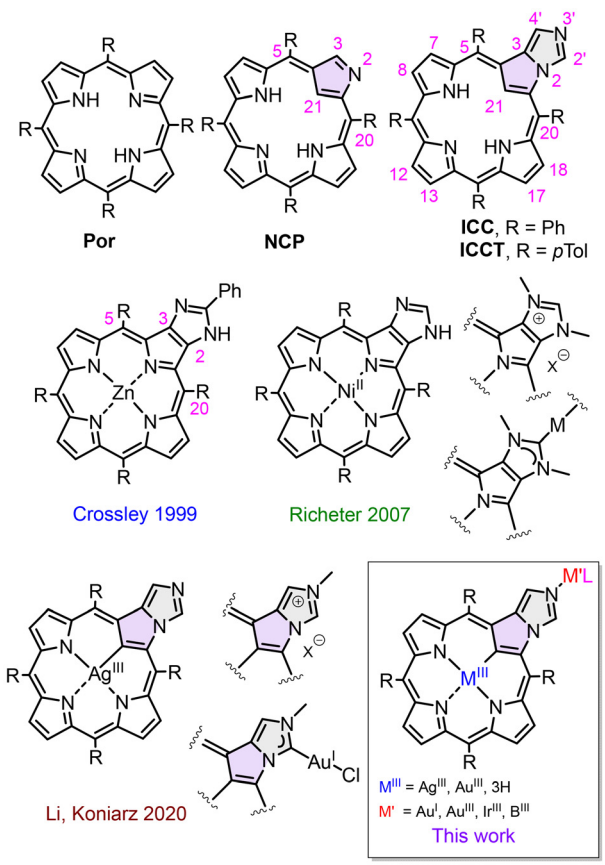

Fig. 1 Imidazole-fused porphyrinoids, their precursors, and complexes.

Department of Chemistry, University of Wrocław, F. Joliot-Curie 14, 50 383 Wrocław, Poland. E-mail: piotr.chmielewski@uwr.edu.pl

given to the structural alterations of the porphyrinoid ring and changes in the redox properties of the complexes caused by the external coordination.

Results and discussion

Synthesis and structure

Although the coordination cores of **NCP** and **ICC** seem to be analogous, there is an essential distinction between these ligands that is related to the presence of a basic center N2 at the perimeter of the macrocycle in the former. Thus, the **NCP** macrocyclic core can act as a mono-, di-, or tris(anionic) ligand forming neutral complexes with divalent or trivalent metal cations, with 2-NH compensating an excess of the negative charge in the case of M^{2+}-**NCP** systems. On the other hand, the imidazole imide-like nitrogen N3′ in **ICC** appears to be unable to hold the proton under neutral conditions. Hence, **ICC** is invariantly a tris(anionic) ligand if the macrocyclic coordination core is concerned, stabilizing trivalent metals and concurrently preserving basic nucleophilic properties of N3′. Thus, we chose a readily obtainable silver(III) complex as a workhorse and common platform in our study of the coordination of the imidazole nitrogen of **ICC**. However, in some instances, we observed here the coordination of the N3′ site in the systems not involving the macrocyclic crevice in ligation. This allowed us to discuss the influence of the macrocyclic ring rigidity, imposed by the coordination of the inert d^8 metal ion, on the overall structure of the bis(metallic) system.

The syntheses were carried out under relatively mild conditions, and the products were characterized by spectroscopic methods, including 1D NMR and 2D homo- and heteronuclear correlation techniques, single crystal X-ray diffraction analyses (XRD), optical spectroscopy, and electrochemical methods (cyclic and differential pulse voltammetry).

ICC-triphenylboroxine adduct. In its compounds, boron(III) prefers trigonal planar or tetrahedral geometry, while macrocyclic oligopyrroles, such as porphyrins and analogues, except subporphyrins and subphthalocyanines,[54,55] offer square-planar, square-pyramidal, or square-bipyramidal environment. Moreover, the low atomic radius of boron excludes simultaneous coordination of relatively rigidly situated four pyrrole nitrogens without considerable deformation of the whole aromatic ring. Despite all that, many of the boron complexes have been reported for porphyrins and corroles comprising one or two B^{III} in the macrocyclic cavity.[56–62] In all tetrapyrroles and expanded porphyrins, *i.e.*, porphyrinoid consisting of five or more pyrrole subunits, the macrocycle acts as a dipyrrin-like ligand, thus involving only two nitrogen donors in a six-membered chelate ring. In several instances, such a coordination mode gives rise to a system containing two borons inside the coordination core.[56,57,59,60] Syntheses of all these systems involve boron trihalides, organoboronic acids or dichlorides, as well as boronic esters, as the sources of the central atom.[58] Preparation of the boron complex of **ICC** was attempted in a reaction of its free base with chlorophenyl boron in refluxing toluene under a blanket of N_2 for 90 min. Such a synthetic method has been successfully applied for intraannular phenyloborylation of **NCP**.[63] To our surprise, the reaction resulted in an unexpected adduct involving imidazole nitrogen in a binding with the boron atom of the six-membered triphenylboroxine ring (Scheme 1). The trialkyl- or triarylboroxine, *i.e.*, organoboronic anhydrides,[64–66] are usually obtained by dehydration of boronic acids; thus, the presence of $(BOPh)_3$ in the current synthesis implies hydrolysis of $PhBCl_2$ in the early stage of the reaction, likely by the traces of water present in the reaction mixture. The composition of the complex was recognized by HRMS and NMR and confirmed by XRD (Fig. 2). The asymmetric unit of the crystal consisted of two molecules,

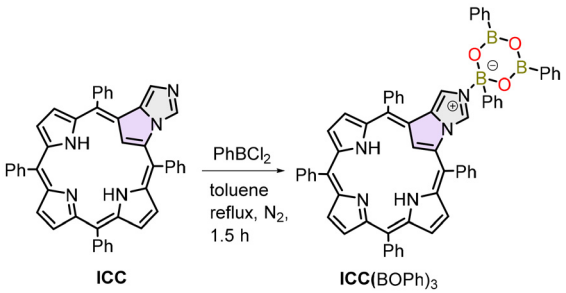

Scheme 1 Synthesis of triphenylboroxine adduct of **ICC**.

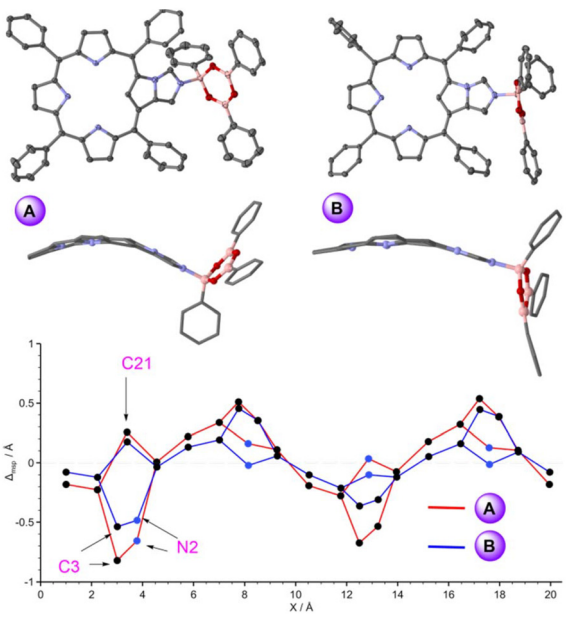

Fig. 2 Molecular structures of the triphenylboroxine adduct of **ICC** based on XRD. The two symmetry-independent molecules are presented separately as molecule A and molecule B. In front views (top, 50% probability displacement ellipsoids), all hydrogens were removed. In the stick side views (mid), the *meso*-phenyls were removed for clarity. In the bottom line, the atom displacements from the porphyrin mean plane calculated[67] from XRD data are presented for both molecules. The error of the distance estimations is ≤0.01 Å.

Table 1 Analyses of the out-of-plane displacements of the porphyrin ring calculated by means of PorphyStruct[67] based on SCXRD structures

Compound	Doming [Å]	Saddling [Å]	Ruffling [Å]	WavingX [Å]	WavingY [Å]	Propellering [Å]	D_{oop}[a] [Å]	DH_1[b] [°]	DH_2[c] [°]	d_{ext}[d]
NCP[e]	0.196	1.360	−0.070	0.259	−0.055	0.040	1.465	27.0	—	—
ICC[f]	0.000	0.000	0.000	−0.147	0.369	−0.001	0.457	16.6	7.5	—
ICC$(PhBO)_3$ **A**	−0.441	−1.620	0.576	−0.155	0.042	0.004	1.817	31.8	3.3	3.116
ICC$(PhBO)_3$ **B**	0.025	1.185	0.260	0.224	0.025	0.020	1.289	21.2	1.2	2.188

[a] Total out-of-plane distortion, ±0.01 Å. [b] Dihedral angle (±0.5°) between the mean plane defined by all non-hydrogen atoms of the macrocyclic ring except C21, N2, and C3, and the mean plane of the *confused* pyrrole. [c] Dihedral angle (±0.5°) between the mean planes of the confused pyrrole and fused imidazole rings. [d] Distance between coordinated boron and the mean plane defined by C21, N22, N23, and N24. [e] X-ray data taken from ref. 2. [f] X-ray data taken from ref. 74.

both strongly deviating from the planarity of the macrocycle. The deformations were analyzed by means of the *PorphyStruct* application,[67] which is based on the normal-coordinate structure decomposition (NSD) approach.[68,69] The results were collected in Table 1 along with the analogous data calculated for **NCP** and **ICC** free bases, for comparison. Both molecules of **ICC**$(PhBO)_3$ exhibited strong saddling deformation with some contribution of doming and ruffling, which are all more pronounced in molecule **A**. Significantly, these deformation modes are completely absent in the solid structure of the starting **ICC** free base. The dihedral angles between the macrocycle mean plane and that of *confused* pyrrole (DH_1) are also considerably higher than in the case of **ICC**, though close to that of **NCP** free base. The fused pyrrole-imidazole system was essentially planar in both **A** and **B**, as it can be inferred from the low values of DH_2, *i.e.*, dihedral angles between the mean planes of these rings (Table 1). The boroxine rings were also planar with mean deviations of 0.05 and 0.06 Å for molecules **A** and **B**, respectively, and a maximum deviation of 0.09 Å for both molecules. The dihedral angles between the boroxine ring and the imidazole mean plane were 74.0° for **A** and 70.1° for **B**. The major difference between the molecules arose from various orientations of the phenyl rings with respect to the boroxine ring in **A** and **B**. In molecule **A**, the aryl rings at the trigonal borons were roughly coplanar with the B_3O_3 moiety, with dihedral angles of 12.3° and 5.7°, and the ring at the pyramidal boron is nearly perpendicular to the boroxine ring with a dihedral angle of 87.3°. Conversely, in molecule **B**, no such "perpendicular" phenyl ring occurred, and the dihedral angle between the boroxine mean plane and the aryl ring at the pyramidal boron is only 40.2°. In comparison, those of phenyls at the trigonal borons are slightly higher than in **A** (17.4° and 18.3°). Two independent molecules have been observed in the structure of 4-picoline adducts with $(4\text{-}MeC_5H_4BO)_3$,[70] although no such strong difference in the respective dihedral angles occurs there. For the pyridine adduct with $(PhBO)_3$, only one type of molecule has been observed in the crystal.[64] No organoboroxine adduct with imidazole has been reported to date. The O–B–O ring angle at the tetrahedral boron was 112.7(2)° for **A** and 113.8(2)° for **B**, while those at the trigonal borons varied from 120.8(2)° to 121.2(2)°. The B–O bond distances were spread from 1.350(3) Å to 1.468(2) Å in **A** and from 1.343(3) Å to 1.464(3) Å in **B**. The B–C distances for tetrahedral borons were considerably longer (1.612(3) and 1.607(3) Å) than those for the trigonal borons (from 1.553(4) to 1.569(3) Å). These structural features are comparable to those observed previously for the organoboroxine adducts with pyridines and their derivatives.[64,70–72] In molecule **B**, the unique B–N distance (1.639(3) Å) was in the range of the distances observed previously for the other adducts (1.635(4)–1.661(4) Å) but considerably shorter bond length of 1.605(2) Å was obtained for molecule **A**. Likely, the distinct arrangement of the phenyl ring in this molecule diminished repulsion of the boroxine and *meso*-aryls of the **ICC** moiety allowing for closer contact of imidazole and boron. Apparently, the different arrangements of the substituents at the triphenylboroxine caused the changes in the crystal packing for **ICC**$(PhBO)_3$, inducing distinct deformations of the macrocycle. Both molecules were chiral owing to the prochiral structure of the macrocycle and differentiation of the porphyrin faces, but the compound crystallized in the centrosymmetric group $P\bar{1}$ as a racemate.

The ^{1}H NMR study indicated persistence of the adduct in solution and fluxional character of **ICC**$(PhBO)_3$. Pyrrole β-proton signals were downfield shifted by about 0.1 ppm with respect to the **ICC** free base. At the same time, imidazole H2′ and H4′ resonated at, respectively, 0.32 and 0.23 ppm higher chemical shifts than in the parent ligand. On the other hand, the signal of 21-CH appeared at δ −5.76 ppm in the adduct, indicating it was upfield shifted by 0.23 ppm compared to the free **ICC**. Apart from the changes in the chemical shifts observed for the signals of the porphyrinoid, there were two broad resonances at δ 7.40 (*ortho*-H) and 7.96 ppm (*meta*- and *para*-H) with a total relative intensity of 15H, diagnostic for the presence of $(PhBO)_3$ in solution. However, the observed lack of differentiation of the phenyl signals placed in the magnetically distinct sites, *i.e.*, at tetrahedral and trigonal borons, strongly suggested a chemical exchange that is fast in the NMR time scale above 250 K (Fig. 3). Similar dynamics in solution has been observed and analyzed for $(PhBO)_3$(7-azaindole)[71] and for the adducts of other tris(aryl)boroxine with amines.[73] The averaging of the chemical shifts indicated a fast change of the boron atom involved in the coordination of the imidazole nitrogen, and thus, a highly labile character of the complex. Moreover, upon crystal growing of **ICC**$(PhBO)_3$, we obtained from the mother liquor (DCM/hexane) another crystal that was colorless and was identified by XRD as that of free $(PhBO)_3$ occurring by a decomposition of the adduct, in line with its labile character.

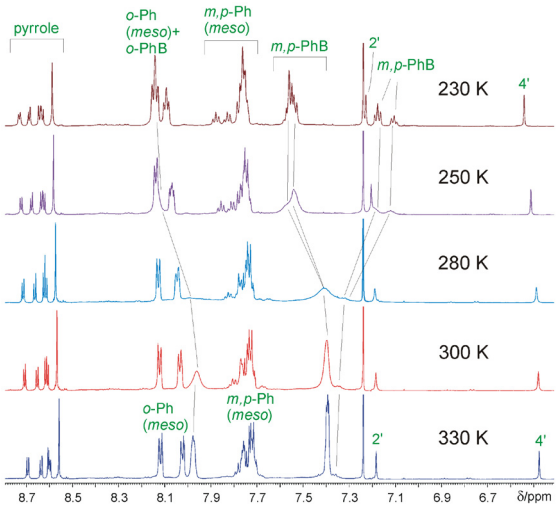

Fig. 3 High-shift parts of the ^{1}H NMR spectra ($CDCl_3$) of **ICC**$(PhBO)_3$ recorded at the specified temperatures.

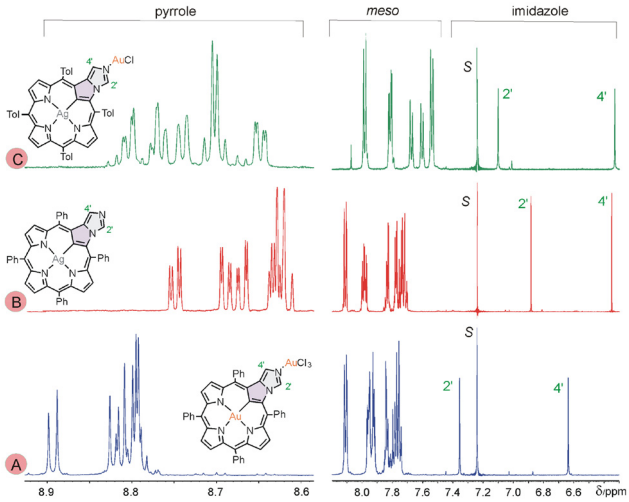

Fig. 4 Low-field regions of the ^{1}H NMR spectra (300 K, $CDCl_3$) of Au**ICC**$AuCl_3$ (A), Ag**ICC** (B), and Ag**ICC**AuCl (C). s = a residual $CHCl_3$ signal.

Gold complexes. The imidazocarbachlorin gold(III) complex Au**ICC**$AuCl_3$ was obtained by reacting potassium tetrachloroaurate(III) as a metal source in the reaction with the **ICC** free base. The reaction was carried out in refluxing benzene for 18 h under a blanket of N_2 in the presence of solid potassium carbonate as a proton scavenger (Scheme 2). The chromatographic workup and crystallization resulted in the deep red product with 71% yield. ^{1}H NMR consisted of six doublets of pyrrole β-protons, several multiplets of phenyl protons, and imidazole H2′ and H4′ signals. No 21-CH or 22,23-NH resonances were present, in line with the coordination of the metal within the porphyrin core. The pyrrole and imidazole signals were shifted downfield with respect to those observed in **ICC** free base. The spectrum resembled that of Ag**ICC** reported previously[54] (Fig. 4B) except for the lack of additional splitting of pyrrole signals due to ^{1}H-^{107,109}Ag coupling and more pronounced downfield shift of the imidazole signals of Au**ICC**$AuCl_3$ (Fig. 4A).

The XRD analysis confirmed the structure of the complex, revealing the presence of two gold ions: one internally coordinated by the **ICC** macrocyclic core, and the other bound to the imidazole nitrogen and three chlorides (Fig. 5).

The high efficiency of the gold insertion into the coordination core of the carbaporphyrinoid upon application of K

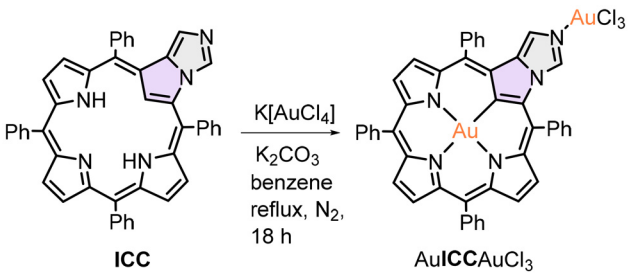

Scheme 2 Synthesis of bis[gold(III)] complex of **ICC**.

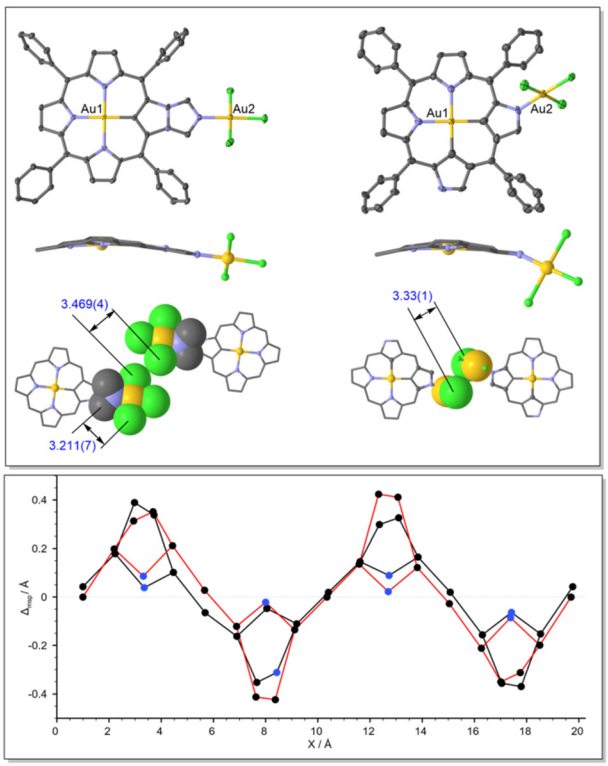

Fig. 5 Upper box: Molecular structures based on XRD analyses (50% displacement ellipsoids) of Au**ICC**$AuCl_3$ (top, left column) and Au**NCP**$AuCl_3$ (right column). All hydrogens are omitted. In the ball-and-sticks representations of the molecule side views (mid), all *meso* phenyls are also removed for clarity. The bottom line presents part of the packing diagrams showing Cl-Cl intermolecular contacts in both crystals. Lower box: the atom displacements from the porphyrin mean plane calculated[67] from XRD data of Au**ICC**$AuCl_3$ (black sticks) and Au**NCP**$AuCl_3$ (red sticks). The error of the distance estimations is ≤0.01 Å.

[$AuCl_4$] prompted us to repeat that synthetic approach for unaltered **NCP**. Although Au**NCP** was obtained in 2008 by Furuta and co-workers,[23] the gold(III) insertion by means of $Au^{I}(Me_2S)Cl$ as a metal source requires activation of the porphyrin by bromination of the inner carbon C21. That, in turn, results in a partial inversion of the *confused* pyrrole and formation of the N-fused porphyrin,[75] reducing the metalation yield. In our hands, the reaction of **NCP** with potassium tetrachloroaurate (III) proceeded smoothly in refluxing dichloromethane in the presence of a proton scavenger (solid K_2CO_3), giving rise to the product containing two gold(III) ions (Scheme 3). XRD and NMR (Fig. 5 and 6) verified the formation and composition of the complex. Furthermore, the bis(gold(III)) complex Au**NCP**$AuCl_3$ was shown to undergo facile demetallation at the external coordination site, efficiently giving rise to Au**NCP**,

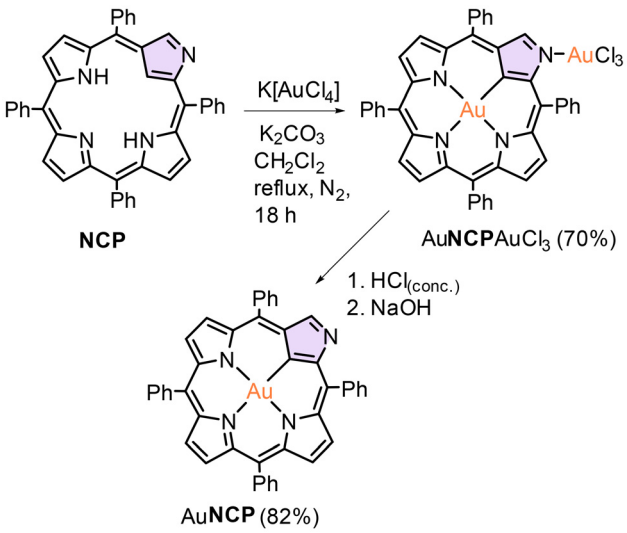

Scheme 3 Synthesis of bis[gold(III)] complex of **NCP**.

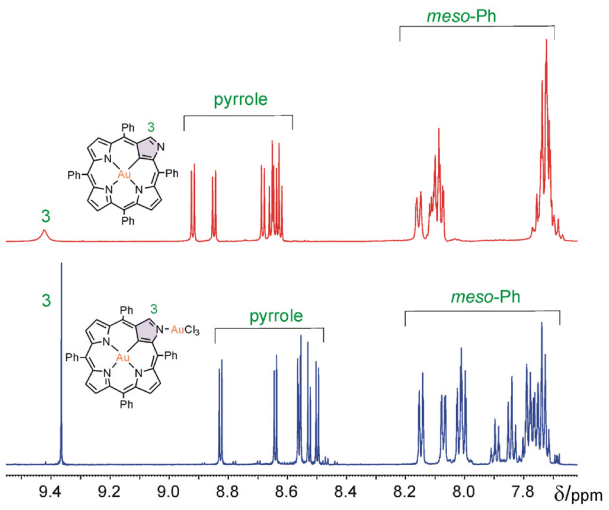

Fig. 6 Low-field regions of the ^{1}H NMR spectra (300 K, $CDCl_3$) of Au**NCP**$AuCl_3$ (bottom), and Au**NCP** (top).

containing gold(III) only in the porphyrin core (Scheme 3). That species was identical to that obtained by Furuta *et al.*, as we established based on ^{1}H NMR (Fig. 6). Interestingly, despite rather harsh conditions applied for the demetallation, *i.e.*, concentrated hydrochloric acid, the carbaporphyrinoid gold(III) complex Au**NCP** remained intact, which indicated a high thermodynamic and kinetic stability of this species. Conversely, the analogous silver(III) **NCP** complex can be easily demetallated under such conditions. On the other hand, the **ICC** bis[gold(III)] complex, Au**ICC**$AuCl_3$, appeared to be less robust than its NCP counterpart and decomposed into many unidentified products upon attempted external demetallation with HCl.

Both bis[gold(III)] complexes indicated similar structural features of the macrocyclic and external chromophores. For Au**ICC**$AuCl_3$ the inner Au1–N bond lengths were 2.030(5), 2.059(5), and 2.036(5) Å while the Au1–C21 distance was 2.004 (6) Å. For the external Au2, the distances with chorines were 2.270(2), 2.262(2), and 2.270(2) Å, and the unique Au2–N was 2.0254(5) Å. For Au**NCP**$AuCl_3$, due to two-fold disorder, only a rough estimation of the average inner Au1–N/C bond length of 2.04 Å was available, and the external Au2–Cl lengths were 2.29 (1), 2.201(8), and 2.31(1) Å with an Au2–N distance of 2.00(1) Å. The average displacement of the donor atoms from the Au1CNNN mean plane was about 0.06 with the metal lying 0.01 Å over that plane in Au**ICC**$AuCl_3$. In comparison, the respective displacements were estimated as 0.05 Å and 0 Å in Au**NCP**$AuCl_3$, indicating effective planarity of the metal environment in both macrocyclic complexes. Also, Au2ClClClN chromophores were essentially planar in both species, with average displacement of chlorines and nitrogen in Au**ICC**$AuCl_3$ of 0.07 but 0.03 and 0.01 Å, respectively, in Au**NCP**$AuCl_3$. The tetrapyrrole ring in both complexes was saddle-shaped (Fig. 5, Table 2). However, a total deviation from the mean plane D_{oop} was slightly higher for Au**NCP**$AuCl_3$, and so were the individual displacements from the mean plane of the macrocyclic atoms (Fig. 5). Likely, the shorter distance between the macrocycle and the external $AuCl_3$ moiety coordinating directly to the *confused* pyrrole may be responsible for the higher deformation of the ring. It is definitely more space for such a moiety in Au**ICC**, which may be inferred from the lower value of the dihedral angle between the mean planes of chromophores Au1CNNN and Au2ClClClN in Au**ICC**$AuCl_3$ (37.8°) than in Au**NCP**$AuCl_3$ (67.7°). The internal and external chromophores cannot be coplanar with each other due to the repulsion between the chlorides and the imidazole carbons and hydrogens (C2′H and C4′H) in Au**ICC**$AuCl_3$. However, a stronger repulsion is observed for the analogous **NCP** complex. The presence of an aryl substituent at the adjacent *meso* position (C20) in Au**NCP**$AuCl_3$ pushes the gold(III)–trichloride plane in a position that is almost perpendicular to the plane of the macrocycle. For both complexes, intermolecular interaction in the solid state was inferred from an appropriate orientation of the interacting molecules as well as from the Cl–Cl distances observed in both crystal structures (Fig. 5) that were shorter than the sum of the chlorine van der Waals radii (3.5 Å).

Table 2 Analyses of the out-of-plane displacements for the porphyrin ring in silver(III) and gold(II) complexes calculated by means of PorphyStruct[67] based on SCXRD structures

Compound	Doming [Å]	Saddling [Å]	Ruffling [Å]	WavingX [Å]	WavingY [Å]	Propellering [Å]	D_{oop}[a] [Å]	DH_1[b] [°]	DH_2[c] [°]	d_{ext}[d] [Å]	AN_{ext}[e]
Au**NCP**AuCl$_3$	0.000	1.173	−0.001	−0.107	0.103	−0.017	1.193	8.8	—	1.03	160.2(8)
Au**ICC**AuCl$_3$	−0.019	−1.059	−0.069	−0.085	0.077	0.003	1.072	9.7	2.5	0.99	178.3(3)
Ag**ICCT**AuCl	0.080	−1.214	0.267	0.031	−0.033	0.007	1.252	11.1	1.7	0.61	172.7(3)
Ag**ICC**IrCp*Cl$_2$	0.149	0.757	−0.063	0.056	−0.110	0.011	0.810	12.0	4.3	2.143	162.5(1)
Ag**ICCMe**AuCl[f]	−0.055	−1.417	−0.513	0.053	−0.140	−0.067	1.528	14.5	5.4	2.078	

[a] Total out-of-plane distortion. The error of the distance estimations is ≤0.01 Å. [b] Dihedral angle (±0.5°) between the mean plane defined by all non-hydrogen atoms of the macrocyclic ring except C21, N2, and C3, and the mean plane of the *confused* pyrrole. [c] Dihedral angle (±0.5°) between the mean planes of the confused pyrrole and the fused imidazole rings. [d] Distance between the externally coordinated metal atom and the mean plane defined by internal chromophore MC21N22N23N24. [e] An angle between C21–N_{ext} and N_{ext}–M directions. [f] X-ray data taken from ref. 74.

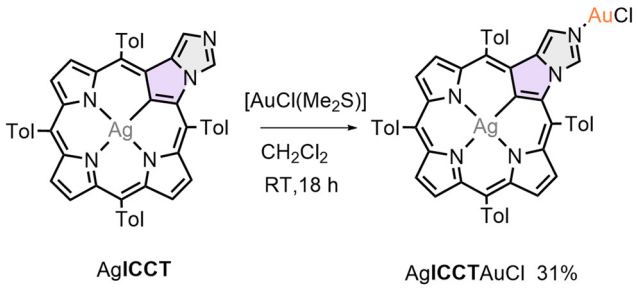

Ag**ICCT** Ag**ICCT**AuCl 31%

Scheme 4 Synthesis of gold(I) complex of Ag**ICCT**.

Another gold complex was obtained in the reaction of silver (III) **ICCT** complex with [AuCl(Me$_2$S)]. The mix-metal complex containing trivalent silver and monovalent gold was formed under mild conditions (Scheme 4). The structure of this species was evaluated based on the XRD analysis (Fig. 7). The Au1–N and Au1–Cl1 bond lengths (1.993(7) and 2.244(2) Å, respectively) are slightly shorter than those observed for Au**ICC**AuCl$_3$ or Au**NCP**AuCl$_3$. ^{1}H NMR spectrum indicated the presence of a silver atom in the porphyrin coordination core by showing split pyrrole proton signals due to H–Ag spin–spin coupling ($^4J_{AgH}$ = 1.5 Hz).† In the crystal lattice of Ag**ICCT**AuCl, formation of a dimer was observed with mutual interaction of the gold ion belonging to one of the monomers with the β-pyrrole carbons C12 and C13 of the other monomer (Fig. 7A). The distances 3.185(7), 3.139(8), and 3.089 for Au1–C12, Au1–C13, and the Au–(C12═C13) centroid, respectively are lower than the sum of the van der Waals radii and strongly suggest the presence of a non-covalent interaction of the electron-rich metal ion and ethylene-like moiety in **ICC**. Deviation from planarity of the macrocycle was significantly more substantial in Ag**ICCT**AuCl than that observed for bis[gold(III)] systems (Table 2), involving doming and ruffling of the ring apart from a more pronounced saddling. That may be the result of the crystal packing forces, mainly the dimer formation in the crystal lattice of Ag**ICCT**AuCl. On the other hand, in all these complexes comprising externally coordinated gold(I/III) ion, the macrocycle displayed less pronounced deformation than that of the previously reported

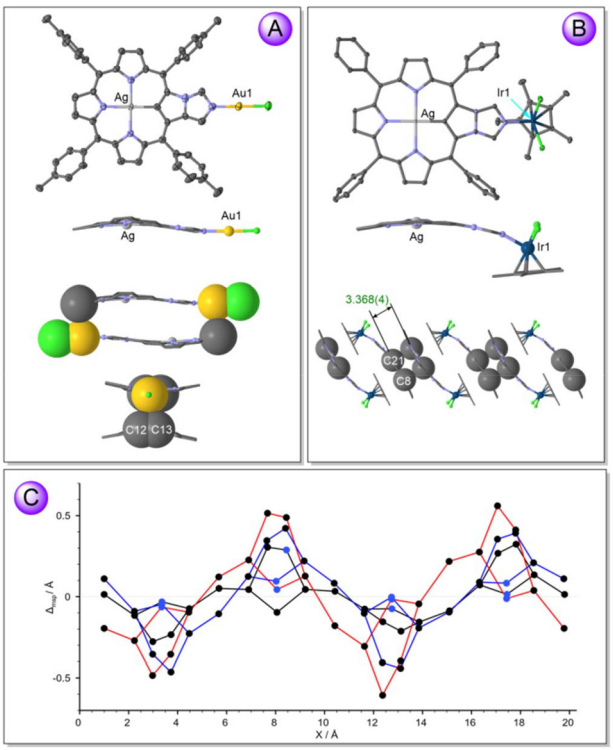

Fig. 7 Panel A: Molecular structure based on XRD analyses (50% displacement ellipsoids) of Ag**ICCT**AuCl (top), ball-and-sticks representation of side view (mid), and two views of the fragment of crystal packing with gold and interacting carbon atoms depicted with space-filling representations (bottom). Panel B: Molecular structure based on XRD analyses (50% displacement ellipsoids) of Ag**ICC**IrCp*Cl$_2$ (top), ball-and-sticks representation of side view (mid), and a fragment of crystal packing with interacting carbon atoms depicted with space-filling representations (bottom). All hydrogens are omitted. In the ball-and-sticks representations of the molecule, all *meso*-phenyls are also removed for clarity. Panel C: The atom displacements from the porphyrin mean plane calculated[67] from XRD data of Ag**ICCT**AuCl (black sticks), Ag**ICC**IrCp*Cl$_2$ (blue sticks), and Ag**ICCMe**AuCl (red sticks).[74] The error of the distance estimations is ≤0.01 Å.

† ^{1}H NMR spectra of certain fractions collected upon the column chromatography of Ag**ICC**AuCl comprised, apart from the resonances of the silver(III) complex, another set of the weaker signals (about 20% of the integral intensity of the major component) that may be assigned to the Au**ICC**AuCl or Au**ICC**.

system,[74] where gold(I) chloride is bound to C2′ of *N*-methylated imidazole in Ag**ICCMe** acting as N-heterocyclic carbene ligand (Fig. 1, 7C and Table 2). It may be a result of the steric congestion in the region of external metal coordination in Ag**ICCMe**AgCl, causing deformation of the ring due to repulsion between the AuCl moiety and the aryl substituent at the *meso*-position C5. No such overcrowding occurs in the molecules consisting of N-coordinating imidazole of Ag**ICC** or Au**ICC**.

Iridium(III) complexes. We have shown recently that the external nitrogen of **NCP** and some of its complexes acting as *ortho*-metallated ligands can be involved in the coordination of late transition metals such as Ru^{III}, Rh^{III}, and Ir^{III}.[41] Since *ortho*-metalation requires a significant deviation of the *confused* pyrrole from the mean porphyrin plane, no such coordination mode is possible for Ag**NCP** or Au**NCP** where that pyrrole is firmly held in plane by C21 σ-bonding to the metal inside the porphyrin core. On the other hand, **ICC** and Ag**ICC** comprise the well-exposed external donor of the fused imidazole and, thus, they can act as monodentate ligands, leaving enough free space for the whole coordination sphere of the external metal. We decided to synthesize and characterize iridium(III) complexes using $[Ir(Cp^*)Cl_2]_2$ as a metal source that introduces a rather voluminous tetramethylcyclopentadienyl ligand and two chlorides, to check the coordination properties of the imidazole donor site under the apparent conditions of steric overcrowding. Both for "empty" **ICCT** and for silver(III) complex Ag**ICC**, the reaction proceeded efficiently in de-aerated dichloromethane at room temperature (Scheme 5). The products were separated and purified only by crystallization and characterized by NMR (Fig. 8). For both systems, the presence of the externally coordinated IrCp* moiety was inferred from an intense signal of methyls of the pentamethylcyclopentadienyl ligand, appearing in ^{1}H NMR spectrum at about δ 1.55 ppm, apart from the dissolved water signal occurring in this region. The signals were assigned to

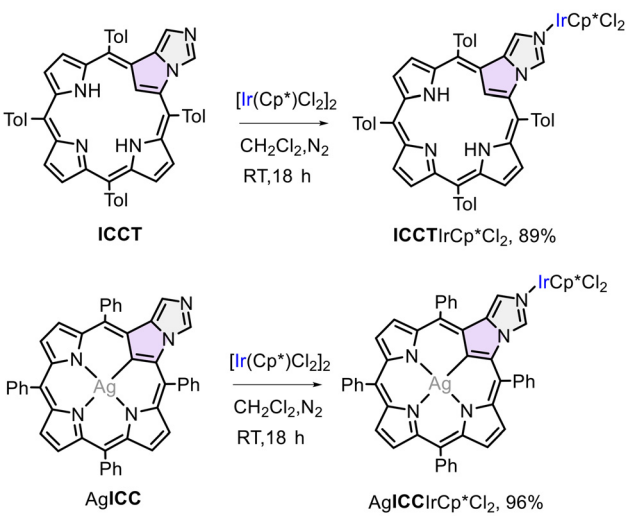

Scheme 5 Synthesis of iridium(III) complexes of **ICCT** and Ag**ICC**.

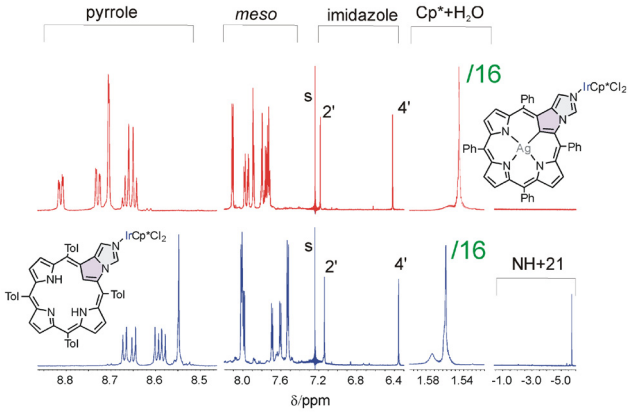

Fig. 8 Selected regions of ^{1}H NMR spectra (300 K, $CDCl_3$) of **ICCT**IrCp*Cl_2 (bottom), and Ag**ICC**IrCp*Cl_2 (top). In both spectra, the intensity was divided by a factor of 16 in the region centered at 1.55 ppm. s = a residual $CHCl_3$ signal.

the Cp* methyls by the appropriate correlations observed in HSQC and HMBC experiments, and ascribed to the complexes by the correlations with imidazole protons in the ROESY spectra (Fig. S21–S24 and S27–S30 in SI). The silver(III) inside the macrocycle was identified by the additional splitting of the pyrrole proton resonances due to Ag–H coupling in the ^{1}H NMR of Ag**ICC**IrCp*Cl_2. On the other hand, the lack of any metal ion inside the porphyrin core in **ICCT**IrCp*Cl_2 was deduced from the presence of the sharp singlet of 21-CH at δ −5.73 ppm and a very broad degenerated signal of 22,23-NH at δ −2 ppm. These features were absent in the proton spectrum of Ag**ICC**IrCp*Cl_2 (Fig. 8). Composition of **ICCT**IrCp*Cl_2 was confirmed by ESI HRMS (1072.3688, calc. for $C_{50}H_{39}ClIrN_8C1_{10}H_{15}$; $[M - Cl]^+$, exp. 1072.3677), while for Ag**ICC**IrCp*Cl_2 the structure was evaluated from the single crystal XRD (Fig. 7B). The porphyrin ring appeared to be least deviated from planarity among the systems analyzed in this work with predominately saddle-shaped type displacement (Table 2 and Fig. 7C). Ag1–N distances within the porphyrin core were 2.039(3), 2.066(2), and 2.048(3) while Ag1–C21 bond length was 2.019(2) Å. The chromophore is essentially planar with maximum deviations of the donor atoms from the AgCNNN mean plane of 0.01 Å and 0.03 Å for the silver central atom. Iridium environment adopted the piano-stool type of structure with Ir1–Cl distances of 2.3900(7) and 2.4021(8) Å and Ir1–N bond length 2.090(2) Å which were comparable to those observed for the *ortho*-metallated **NCP** complexes (2.060(4)–2.066(5) Å for Ir–N and 2.420(1)–2.460(1) for Ir–Cl)[41] or in dimeric $[IrCl_2Cp^*]_2$ (Ir–$Cl_{terminal}$ 2.392(4) Å).[76] The Ir1–C(cyclopentadienyl) distances in Ag**ICC**IrCp*Cl_2 varied from 2.131(3) to 2.168(3) with the shortest bond eclipsed that of Ir1–N. These distances were significantly shorter than in *ortho*-metallated systems (2.187(6)–2.198(3) Å)[41] and comparable to the average bond length observed in $[IrCl_2Cp^*]_2$ (2.132 Å).[76] In the crystal lattice of Ag**ICC**IrCp*Cl_2, the molecules interacted by the π–π stacking forming dimers with the intermolecular C21–C8 distances of 3.367(4) Å (Fig. 7B). The cyclopentadienyl rings

were situated over the macrocycle of the other subunit of the dimer and the mean plane of the AgCNNN chromophore and mean plane of the cyclopentadienyl are nearly parallel with dihedral angle of 4.7°.

Situation of the external coordination site. The analysis of the effect of the external coordination on the shape and deformation of the porphyrin ring by the normal-coordinate structure decomposition may be accompanied by a discussion of the influence of the macrocycle on the environment of the external central atom. The systems on hand allowed comparison of linear, square-planar, tetrahedral, and piano-stool types of geometries of the central atom subjected to coordination by the same monodentate N-ligand composed of the pyrrole-fused imidazole. The arrangement of the external coordination center and the macrocyclic chromophore may be of importance for the energy and electron transfer between these sites and for modification of their potential catalytic activity. To compare those complexes regarding the situation of the external atom with respect to the porphyrin ring, we used as an indicator d_{ext} (Tables 1 and 2), defined as a distance between the external central atom (B^{III}, Au^{III}, or Ir^{III}) and the mean plane of the porphyrin chromophore (MCNNN, M = none, Ag^{III}, or Au^{III}). For the analysis, three structural parameters were taken: a dihedral angle between the mean plane defined by all non-hydrogen atoms of the macrocyclic ring except C21, N2, and C3 and the mean plane of the *confused* pyrrole (DH_1), dihedral angle between mean planes of the *confused* pyrrole and fused imidazole rings (a "hinge" angle DH_2), and AN_{ext}, an angle between C21–N_{ext} and N_{ext}–M directions (N_{ext} is either N2 in **NCP** or N3′ in **ICC**). Each of these parameters reflects a different deformation leading to some out-of-plane shift of the external central atom. The strongest displacements from the plane were observed for the boron complex in both molecules (Table 1), and that was primarily due to a significant deviation of the *confused* pyrrole from the mean porphyrin plane. In both molecules, the curvature of the fused imidazole coordination was insignificant, as expressed by AN_{ext} = 177.0(1)° and almost coplanar fused rings, although the hinge angle DH_2 was higher in molecule **A**. Among the bis(metalic) complexes, the most pronounced displacement of the external ion from the macrocycle plane was observed for Ag**ICC**IrCp*Cl_2 which was also reflected by the most significant deviation of the *confused* pyrrole (DH_1) and strongest bending of the fused ring system (DH_2) among the N-coordinating systems in Table 2 and meaningful deviation from linearity (AN_{ext} < 180°). As expected, the least displacement took place in Ag**ICCT**AuCl, comprising a linear coordination environment, although about 8°-bending at N_{ext} was observed, likely due to intermolecular interactions in the solid state. Interestingly, for both bis[gold(III)] complexes, the external metals are displaced to a comparable extent, although in the Au**NCP**AuCl_3, the bending of the Au–N direction out of the *confused* pyrrole plane is significant (AN_{ext} ~160°).

Electronic and redox properties

Optical spectra. The shape of the electronic spectra of **ICC** and its complexes remained porphyrin-like with an intense Soret band near 450 nm and three or four weaker Q-bands in a region of 500–700 nm and some broader absorption in the UV region below 300 nm (Fig. 9). The spectra of the bis(metallic) systems were close to each other and resembled that of Ag**ICC**[74] comprising metal ion only in the porphyrin core. Upon external coordination, the Soret-type band at 452 nm was blue-shifted by 3–6 nm while the lowest-energy Q band at 627 nm was also shifted hypsochromically by 10–15 nm, indicating some increase of the HOMO–LUMO gap. The blue shift is even more pronounced when compared to the lowest-energy Q-bands in the spectra of the doubly metallated **ICC** with that of the free base ($\Delta\lambda$ = 80–90 nm), indicating the synergetic effect of internal and external coordination on the optical properties of the porphyrinoid. On the other hand, for the complexes with no metal inside the coordination core, *i.e.* **ICC**$(PhBO)_3$ and **ICCT**IrCp*Cl_2, the changes with respect to the free base **ICC** were marginal with a blue shift in both Soret and Q regions not exceeding 2 nm.

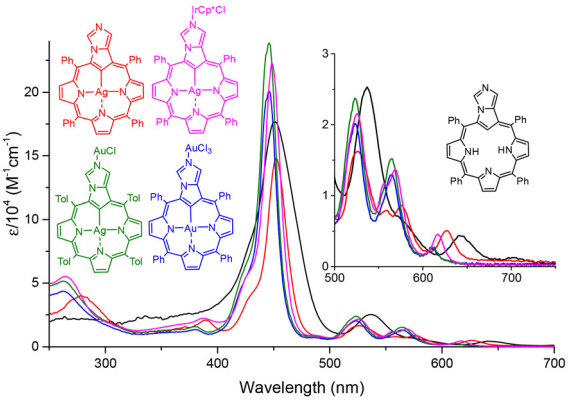

Fig. 9 Electronic spectra of **ICC** (black), Ag**ICC** (red), Au**ICC**AuCl_3 (blue), Ag**ICC**AuCl (green), and Ag**ICC**IrCp*Cl_2 (magenta) in dichloromethane.

Electrochemistry. The electrochemical study was carried out using cyclic (CV) and differential pulse (DP) voltammetry in dichloromethane (Fig. 10 and Fig. S44–S52 in SI). All systems under study were redox active in the electrochemical window from −2.5 to 1.5 V. The selected results of electrochemical measurements are presented in Table 3. The triphenylboroxine adduct of **ICC** exhibited several features in the voltammograms, but all of them were highly irreversible, similarly to **ICC** free base or "empty" **NCP**. Nevertheless, a significant anodic shift of the first oxidation by 0.25 V can be noticed upon boron coordination. For the bis(metallic) systems, at least one reduction and one oxidation were observed. The coordination of the external nitrogen in Ag**ICC** strongly changed redox properties, shifting anodically the first oxidation process by 0.21 V in Ag**ICCT**AuCl (reversible, Fig. 10B) and by 0.13 V in Ag**ICC**IrCp*Cl (irreversible, Fig. 10D), while the reversible first reductions appeared at the potentials of about 0.1 V higher in the voltammograms of both complexes than in those, of Ag**ICCT** or Ag**ICC**. Consequently, the electrochemical HOMO–LUMO gap HLG = $e(E_{Ox1} - E_{Red1})$ increased

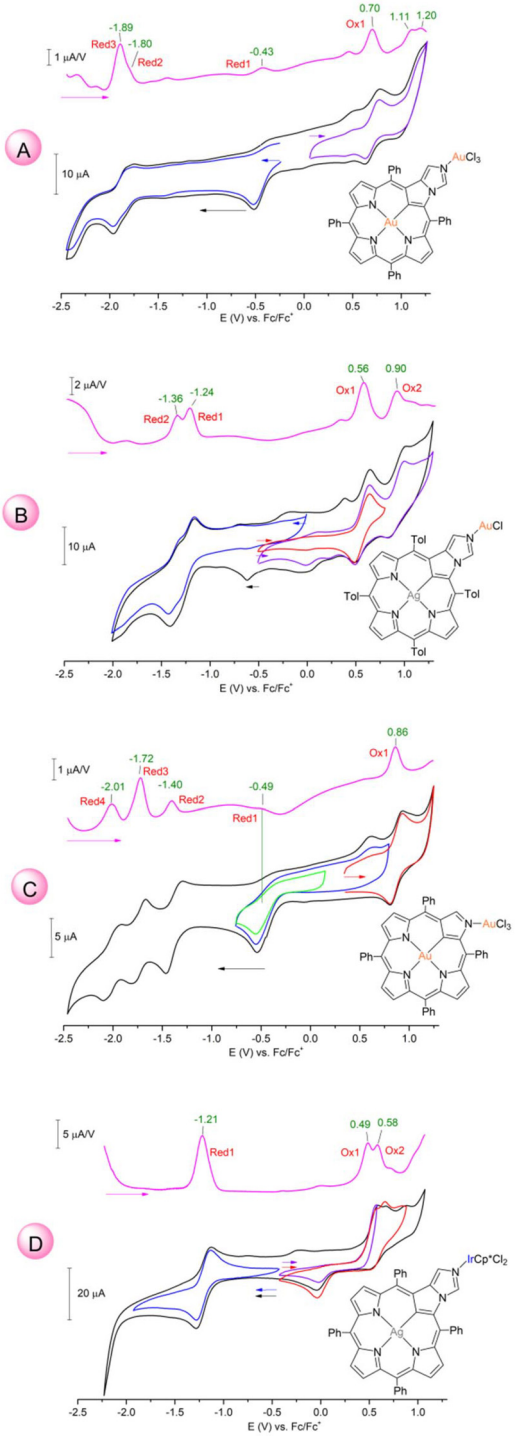

Fig. 10 Cyclic (lower traces) and differential pulse voltammograms (upper traces) for Au**ICC**AuCl$_3$ (A), Ag**ICC**AuCl (B), Au**NCP**AuCl$_3$ (C), and Ag**ICC**IrCp*Cl$_2$ (D) in dichloromethane. The peak potentials in volts (green numbers).

by 0.12 and 0.04 eV, respectively. These redox processes are centred on the porphyrin rather than on the Ag^{III}. However, one of the reversible reductions at −1.36 or −1.24 V for Ag**ICCT**AuCl and one of the oxidations at 0.49 or 0.58 V for

Table 3 Selected electrode potentials for silver(III) and gold(III) complexes of **ICC** and **NCP**

System	E_{Red1} [V]	E_{Red2} [V]	E_{Ox1} [V]	E_{Ox2} [V]	HLG [eV]
ICC[a]	−1.74	−2.23	0.25	0.49	1.99
ICC(BOPh)$_3$[b]	−1.76	−2.25	0.49	0.64	2.25
Ag**ICC**[a]	−1.31		0.36	0.48	1.67
Ag**ICCT**[c]	−1.32		0.35	0.49	1.67
Ag**ICC**AuCl	−1.23	−1.36	0.56	0.90[d]	1.79
Ag**ICC**IrCp*Cl	−1.21		0.49	0.58	1.71
Au**ICC**AuCl$_3$	−0.43[d]	−1.89	0.70	1.11	1.14
Au**NCP**AuCl$_3$	−0.49[d]	−1.40	0.86		1.35
Au**NCP**[e]	−1.54[d]		0.53		2.07

[a] Data from ref. 74. [b] All processes irreversible. [c] Ligand with *p*-tolyl instead of phenyl *meso*-substituents. Data from ref. 74. [d] Irreversible process. [e] Data from ref. 23.

Ag**ICC**IrCp*Cl$_2$ may be due to the processes occurring at the internal or external metal. The voltammograms of Au**ICC**AuCl$_3$ revealed, apart from reversible oxidation and reduction separated by 2.59 V, an irreversible reduction at −0.43 V. Although a more precise estimation was hindered by the process's irreversibility, a rough estimation of the reduction current suggested a two-electron reduction at this potential. The analogous irreversible reduction took place for Au**NCP**AuCl$_3$ at −0.49 V, accompanied by one reversible oxidation at relatively high potential of 0.86 V and three reversible reductions in the potential region below −1.4 V. Considering that these two systems comprised the same set of the internally and externally coordinated metals, the gold(III) reduction in this region was rationally inferred for both Au**ICC**AuCl$_3$ and Au**NCP**AuCl$_3$. The two-electron reduction and irreversible nature of these processes suggested that the AuCl$_3$ moiety serves as the electron acceptor. Upon such reaction, the gold(I) was generated, which was followed by changes in the coordination environment of the metal, *i.e.*, dissociation of the chlorides from the first sphere of Au$^+$, preventing effective re-oxidation at this center. Significantly, for Au**NCP**, only reversible oxidation at 0.53 V and irreversible reduction at −1.54 V have been observed, both assigned to the macrocycle-centered redox processes.[23] Thus, the appearance of the additional redox process upon coordination of the Au^{III} to the external nitrogen of the **NCP** is in line with the assignment of the observed signals to the reduction of the external gold(III). On the other hand, for both "regular" porphyrin and corrole gold(III) complexes, the reversible one-electron metal-centered reductions have been observed at the potentials well above −1 V, and the products were identified by spectroelectrochemistry and EPR.[77,78] Unfortunately, due to the irreversible character of the reductions at about −0.5 V in both of our bis[gold(III)] systems, we were unable to perform any of such decisive experiments.

Conclusions

In conclusion, we have shown here that imidazocarbachlorin can serve as a monodentate ligand in both free-base and

internally metallated forms. Coordination by the externally located imidazole nitrogen affects to some extent the structure of the ligand, and the changes of its shape are much more pronounced for the system with no metal inside the porphyrin core. The fused imidazole is shown to be a part of the coordination sphere of linear, tetrahedral, square pyramidal, and piano-stool geometries. We anticipate that the exposition of the imidazole nitrogen out of the sterically congested region of adjacent *meso*-aryls enables coordination of more than one molecule of **ICC** to the metal ions, thus allowing formation of coordinative dimers or trimers. External coordination influences the optical properties of the porphyrinoid, resulting in a hypsochromic shift of the Soret and Q-bands. Strong absorption of the metalloligands M**ICC** and their redox properties, along with coordination abilities of the external metal centers, may find application in the construction of various catalytic and photocatalytic systems tailored by judicious choice of the internal and external central atoms. Further study on these subjects is underway in our laboratory.

Experimental

Methods and instrumentation

Commercial reagents were used without further purification. Solvents were freshly distilled from the appropriate drying agents or purified under nitrogen with the mBraun MBSPS-800 before use. Column chromatography was performed using silica gel 60 (200–300 mesh ASTM). The NMR spectra were recorded on a Bruker Avance III spectrometer, operating at 500 MHz for ^{1}H and 125 MHz for ^{13}C, or a Bruker Avance III spectrometer operating at 600 MHz for ^{1}H and 150 MHz for ^{13}C. TMS was used as an internal reference for ^{1}H and ^{13}C chemical shifts, and $CDCl_3$ was used as the solvent. Standard pulse programs from the Bruker library were used for homo- and heteronuclear 2D experiments. Mass spectrometry measurements were conducted by using the electrospray ionization technique on a Bruker Daltonics microTOF-Q. Absorption UV/Vis/NIR spectra were recorded by using a Varian Cary 60 and Jasco V-770 spectrophotometers. Electrochemical measurements were performed by means of an Autolab (Metrohm) potentiostat/galvanostat system for dichloromethane solutions with a glassy carbon, a platinum wire, and Ag/AgCl as the working, auxiliary, and pseudoreference electrodes, respectively. Tetrabutylammonium hexafluorophosphate was used as a supporting electrolyte. The potentials were referenced with the ferrocene/ferrocenium couple used as an internal standard. The X-ray diffraction was measured using either XtaLAB Synergy R or Xcalibur, Onyx diffractometers using a copper source of radiation (λ = 1.54184 Å), and collected with a CCD camera. The standard temperature of the measurement was 100 K. The structures were solved using direct methods with SHELXT[79] and refined by the full-matrix least-squares method on all $F2$ data by using the SHELXL[80,81] incorporated in the OLEX2 program.[81] All hydrogen atoms, including those located in the difference density map, were placed in calculated positions and refined as the riding model. The SQUEEZE procedure,[82] was applied for disordered lattice solvent molecules in Ag**ICC**AuCl, Au**NCP**$AuCl_3$, and **ICC**$(BOPh)_3$. Crystallographic details are collected in Tables S1–S5 (SI). Disordered solvent molecules masked with OLEX2 were included in final crystal compositions (structures Au**NCP**$AuCl_3$, Ag**ICC**AuCl, and **ICC**$(BOPh)_3$). Due to partial reduction of the externally attached $AuCl_n$ and consecutive demetallation at 3′, which likely occurred during crystal growing, these fragments were refined with <100% occupancy in structures of Au**ICC**$AuCl_3$ and Ag**ICC**AuCl. In the structure of Au**NCP**$AuCl_3$, maximum around Au1 was assigned as a small disordered gold contribution. Its occupancy was refined to be *ca.* 4%, then was fixed, and the displacement ellipsoid was constrained with EADP to Au1. CCDC 2394665, 2394666, 2394670, 2394671, 2394677 contain supplementary crystallographic data for this paper.

Syntheses and characterizations

Syntheses of precursors. NCP, **ICCT**, and **ICC** ligands, as well as metalloligands Ag**ICCT** and Ag**ICC**, were obtained by the literature methods.[3,74]

Synthesis of ICC(BOPh)$_3$. A sample of **ICC** (0.010 g, 0.0153 mmol), $PhBCl_2$ (40 μL, 0.306 mmol) and toluene (20 mL) were placed in round-bottom flask. The reaction mixture was deoxidized for 20 minutes with N_2, and then heated at the boiling point of the solvent for 1 h under reflux. After that time, the reaction mixture was filtered, the solution was concentrated and applied to a silica gel column. The compound was eluted using 0.5% MeOH in dichloromethane. The collected fraction was evaporated to dryness and recrystallized from the dichloromethane/*n*-hexane system. Yield 8.9 mg (84%).

Selected data for **ICC**$(BOPh)_3$: ^{1}H NMR (600 MHz, $CDCl_3$, 300 K): δ −5.76 (s, 1H, –CH (21)), −1.84 (s, 2H, –NH), 6.51 (s, 1H, (4′)), 7.21 (s, 1H, (2′)), 7.43 (m, 10H, –Ph(B)), 7.77 (m, 12H, (*m*-Ph, *p*-Ph, ArH)), 7.99 (m, 5H, –Ph(B)), 8.05 (d, 4H, $^{3}J_{HH}$ = 7.64 (*o*-Ph, ArH)), 8.15 (d, 4H, $^{3}J_{HH}$ = 7.57 (*o*-Ph, ArH)), 8.59 (m, 2H, (pyrrH)), 8.63 (m, 2H, (pyrrH)), 8.67 (AB, 1H, $^{3}J_{HH}$ = 4.88, (pyrrH)), 8.72 (AB, 1H, $^{3}J_{HH}$ = 4.95, (pyrrH)). ^{13}C NMR (150 MHz, $CDCl_3$, 300 K): δ 155.7, 141.6, 140.1, 138.2, 138.1, 138.0, 137.8, 136.9, 134.5, 134.4, 133.3, 132.7, 130.4, 130.3, 130.2, 129.3, 128.9, 128.2, 127.4, 127.3, 127.1, 126.9, 126.6, 126.3, 125.9, 121.1, 119.4, 114.5, 111.8, 103.7. UV-vis (CH_2Cl_2) λ [nm] ($\varepsilon/10^4$ [M^{-1} cm^{-1}]) = 334 (1.08), 350 (sh), 368 (1.19), 380 (sh), 448 (7.98), 509 (sh), 534 (1.09), 562 (sh), 577 (0.32), 617 (sh), 640 (0.24), 673 (sh).

Synthesis of AgICCIrCp*Cl$_2$. A sample of Ag**ICC** (0.020 g, 0.026 mmol), dichloro(pentamethylcyclopentadienyl)iridium (III) dimer (0.013 g, 0.054 mmol), and dichloromethane (10 mL) were placed in the two-necked flask. The reaction mixture was deoxidized for 20 minutes with N_2, and then the solution was stirred at room temperature for 18 h. After that time, the reaction mixture was filtered and concentrated. Then *n*-hexane was added, and the solution was allowed to crystallize at room temperature. The collected precipitate was washed with a small amount of methanol. Yield 28 mg (96%).

Selected data for Ag**ICC**IrCp*Cl_2: ^{1}H NMR (600 MHz, $CDCl_3$, 300 K): δ 1.56 (s, 15H, Cp*), 6.44 (s, 1H, (4′)), 7.21 (s, 1H, (2′)), 7.76 (m, 6H, ArH), 7.82 (m, 3H, ArH), 7.91 (m, 3H, ArH), 7.97 (m, 2H, ArH), 8.00 (m, 2H, ArH), 8.13 (d, $^3J_{HH}$ = 7.8 Hz, 4H, ArH), 8.67 (AB, $^3J_{HH}$ = 4.8 Hz, 1H, pyrrH), 8.67 (AB, $^3J_{HH}$ = 4.8 Hz, 1H, pyrrH), 8.73 (d, $^4J_{AgH}$ = 1.2 Hz, 2H, pyrrH), 8.75 ($^3J_{HH}$ = 4.9 Hz, $^4J_{AgH}$ = 0.8 Hz, 1H, pyrrH), 8.83 (dd, $^3J_{HH}$ = 5.0 Hz, $^4J_{AgH}$ = 1.5 Hz, 1H, pyrrH). ^{13}C NMR (150 MHz, $CDCl_3$, 300 K): δ 141.6, 141.5, 140.8, 139.2, 139.0, 138.2, 138.1, 137.5, 137.3, 137.1, 133.9, 133.8, 131.7, 131.2, 130.4, 130.2, 130.1, 129.8, 129.3, 129.2, 128.8, 128.8, 128.3, 127.3, 127.0, 126.8, 124.1, 122.9, 122.5, 122.0, 121.8, 117.2, 115.3, 85.1, 77.4, 77.2, 76.9, 8.9. UV-vis (CH_2Cl_2) λ [nm] (ε/10^4 [M^{-1} cm^{-1}]) = 264 (5.51), 327 (sh), 388 (2.23), 402 (sh), 449 (22.40), 502 (sh), 526 (2.16), 547 (sh), 556 (1.17), 561 (sh), 569 (1.36), 600 (sh), 617 (0.46).

Synthesis of ICCTIrCp*Cl_2. A sample of **ICCT** (0.020 g, 0.03 mmol), dichloro(pentamethylcyclopentadienyl)iridium(III) dimer (0.012 g, 0.054 mmol), and dichloromethane (10 mL) were placed in the two-necked flask. The reaction mixture was deoxidized for 20 minutes with N_2, and then the solution was stirred at room temperature for 18 h. After that time, the reaction mixture was filtered and concentrated. Then *n*-hexane was added, and the solution was left to crystallize. The collected precipitate was washed with a small amount of methanol. Yield 30 mg (89%).

Selected data for **ICCT**IrCp*Cl_2: ^{1}H NMR (600 MHz, $CDCl_3$, 300 K): δ −5.71 (s, 1H, 21-CH), 0.79–(−3.71) (2H, 22-NH, 24-NH), 1.58 (s, 15H, Cp*), 2.68 (m, 9H, (–CH_3)), 2.72 (s, 3H, (–CH_3)), 6.38 (s, 1H, (4′)), 7.16 (s, 1H, (2′)), 7.55 (AA′ XX′, 4H, (*m*-tol, ArH)), 7.63 (AA′ XX′, 2H, (*m*-tol, ArH)), 7.71 (AA′ XX′, 2H, (*m*-tol, ArH)), 8.03 (m, 8H, (*o*-tol, ArH)), 8.57 (m, 2H, pyrrH), 8.60 (AB, $^3J_{HH}$ = 4.7 Hz, 1H, pyrrH), 8.62 (AB, $^3J_{HH}$ = 5.1 Hz, 1H, pyrrH), 8.67 (AB, $^3J_{HH}$ = 4.7 Hz, 1H, pyrrH), 8.69 (AB, $^3J_{HH}$ = 5.1 Hz, 1H, pyrrH). ^{13}C NMR (150 MHz, $CDCl_3$, 300 K): δ 155.4, 140.0, 138.9, 138.7, 138.4, 138.3, 137.9, 137.7, 137.1, 135.4, 134.5, 134.1, 134.0, 133.5, 132.7, 132.5, 131.8, 130.9, 129.5, 127.8, 127.1, 126.9, 126.7, 125.9, 125.7, 121.9, 120.8, 118.7, 111.5, 103.0, 102.9, 100.0, 94.5, 88.3, 86.4, 85.0, 32.1, 29.8, 29.5, 22.8, 21.8, 21.6, 14.2, 9.5, 9.2, 8.7. HRMS (ESI): *m*/*z* 1072.3677 [M − Cl], calcd for $C_{60}H_{54}ClIrN_5$ 1072.3688. UV-vis (CH_2Cl_2) λ [nm] (ε/10^4 [M^{-1} cm^{-1}]) = 341 (1.80), 357 (sh), 450 (11.76), 510 (sh), 533 (1.57), 564 (sh), 574 (0.64), 615 (sh), 636 (0.40), 700 (0.22).

Synthesis of Ag**ICCT****AuCl.** A sample of Ag**ICCT** (*meso-p*-tolyl) (0.010 g, 0.0132 mmol), [AuCl(Me_2S)] (0.0078 g, 0.0264 mmol), and dichloromethane (10 mL) were placed in the two-necked flask. The solution was stirred at room temperature for 18 h. After that time, the reaction mixture was filtered, the solution was concentrated and applied to a silica gel column. The product was eluted as the second, raspberry-orange color fraction (hexane : CH_2Cl_2 – 40 : 60). The collected fraction was evaporated to dryness and recrystallized from the dichloromethane/*n*-hexane system. Yield 4.3 mg (31%).

Selected data for Ag**ICCT**AuCl: ^{1}H NMR (600 MHz, $CDCl_3$, 300 K): δ 2.70 (s, 6H, (–CH_3)), 2.75 (s, 3H, (–CH_3)), 2.76 (s, 3H, (–CH_3)), 6.33 (s, 1H, (4′)), 7.10 (s, 1H, (2′)), 7.56 (AA′ XX′, $^3J_{HH}$ = 7.75 Hz, 4H, (*m*-tol, ArH)), 7.62 (AA′ XX′, $^3J_{HH}$ = 7.9 Hz, 2H, (*m*-tol, ArH)), 7.70 (AA′ XX′, $^3J_{HH}$ = 7.8 Hz, 2H, (*m*-tol, ArH)), 7.83 ($^3J_{HH}$ = 8.0 Hz, 4H, (*o*-tol, ArH)), 8.00 (AA′ XX′, $^3J_{HH}$ = 7.2 Hz, 4H, (*m*-tol, ArH)), 8.67 (AB, $^3J_{HH}$ = 4.7 Hz, $^4J_{AgH}$ = 1.4 Hz, 1H, pyrrH), 8.72 (m, 2H, pyrrH), 8.76 (AB, $^3J_{HH}$ = 4.8 Hz, 1H, pyrrH), 8.79 (m, 1H, pyrrH), 8.82 (AB, $^3J_{HH}$ = 4.8 Hz, $^4J_{AgH}$ = 1.5 Hz, 1H, pyrrH). ^{13}C NMR (150 MHz, $CDCl_3$, 300 K): δ 140.4, 139.5, 139.2, 139.1, 139.0, 138.6, 138.5, 138.4, 138.3, 138.2, 138.1, 137.9, 137.7, 137.5, 135.1, 133.8, 133.8, 133.7, 132.6, 131.3, 131.1, 130.9, 130.7, 130.5, 130.1, 129.8, 129.7, 129.6, 129.3, 128.1, 128.0, 127.3, 127.0, 123.4, 122.8, 122.5, 121.6, 116.0, 115.4, 32.1, 29.8, 29.5, 22.8, 22.0, 21.9, 21.7. UV-vis (CH_2Cl_2) λ [nm] (ε/10^4 [M^{-1} cm^{-1}]) = 373 (1.17) 393 (sh), 428 (14.59), 480 (sh), 514 (1.06), 544 (sh), 557 (0.81), 595 (sh).

Synthesis of Au**ICC****AuCl_3.** A sample of **ICC** (0.050 g, 0.08 mmol), K[$AuCl_4$] (0.09 g, 0.24 mmol), anhydrous K_2CO_3 (0.332 g, 2.4 mmol), and benzene (25 mL) were placed in the two-necked flask. The reaction mixture was deoxidized for 20 minutes with N_2, and then heated for 18 h under reflux. After that time, the reaction mixture was filtered, the solution was concentrated, and applied to a silica gel column. The product was eluted as the first, red fraction (hexane : CH_2Cl_2 – 30 : 70). The collected fraction was evaporated to dryness and recrystallized from the dichloromethane/n-hexane solvent system. Yield 63 mg (71%).

Selected data for Au**ICC**AuCl_3: ^{1}H NMR (600 MHz, $CDCl_3$, 300 K): δ ^{1}H NMR (600 MHz, CDCl3) δ (ppm): 6.66 (s, 1H, (4′)), 7.38 (s, 1H, (2′)), 7.79 (m, 5H, ArH), 7.86 (m, 3H, ArH), 7.94 (m, 4H, ArH), 7.98 (m, 4H, ArH), 8.13 (d, $^3J_{HH}$ = 7.3 Hz, 4H, ArH), 8.82 (m, 3H, pyrrH), 8.83 (m, 2H, pyrrH), 8.91 (AB, $^3J_{HH}$ = 5.1 Hz, 1H, pyrrH). ^{13}C NMR (150 MHz, $CDCl_3$, 300 K): δ 140.8, 140.2, 138.6, 138.3, 137.9, 137.6, 137.5, 137.2, 136.3, 135.8, 133.8, 131.3, 131.1, 130.8, 130.7, 130.5, 130.1, 129.8, 129.6, 129.5, 129.0, 128.8, 128.6, 127.6, 127.5, 127.4, 124.1, 124.0, 122.3, 122.0, 118.6, 117.5, 116.5, 102.7. UV-vis (CH_2Cl_2) λ [nm] (ε/10^4 [M^{-1} cm^{-1}]) = 428 (18.31), 493 (sh), 514 (1.47), 534 (sh), 557 (1.17).

Synthesis of Au**NCP****AuCl_3.** A sample of **NCP**(Ph) (0.062 g, 0.1 mmol), K[$AuCl_4$] (0.113 g, 0.3 mmol), anhydrous K_2CO_3 (0.30 g, 2.17 mmol), and $CHCl_3$ (35 mL) were placed in the two-necked flask. The reaction mixture was deoxidized for 20 minutes with N_2, and then heated for 18 h under reflux. After that time, the reaction mixture was filtered, the solution was concentrated and applied to a chromatography on a silica gel column. The product was eluted as the main fraction (hexane : CH_2Cl_2 – 30 : 70). The collected fraction was evaporated to dryness and recrystallized from the dichloromethane/n-hexane solvent system. Yield 78 mg (71%).

Selected data for Au**NCP**AuCl_3: ^{1}H NMR (500 MHz, $CDCl_3$, 300 K): δ 7.71–7.80 (om, 9H, ArH), 7.83 (om, 2H, ArH), 7.90 (om, 1H, ArH), 8.01 (om, 4H, ArH), 8.06 (om, 2H, ArH), (om, 1H, ArH), 8.15 (om, 2H, ArH), 8.50 (AB, $^3J_{HH}$ = 5.1 Hz, 1H, pyrrH), 8.53 (AB, $^3J_{HH}$ = 5.1 Hz, 1H, pyrrH), 8.55 (AB, $^3J_{HH}$ = 5.1 Hz, 1H, pyrrH), 8.56 (AB, $^3J_{HH}$ = 5.1 Hz, 1H, pyrrH), 8.64 (AB, $^3J_{HH}$ = 5.1 Hz, 1H, pyrrH), 8.83 (AB, $^3J_{HH}$ = 5.1 Hz, 1H, pyrrH),

9.36 (s, 1H, pyrrH). ^{13}C NMR (150 MHz, $CDCl_3$, 300 K): δ 160.7, 142.7, 142.6, 141.1, 141.0, 139.7, 139.4, 137.9, 136.4, 135.9, 135.7, 134.4, 133.65, 133.61, 133.58, 133.0, 132.8, 132.5, 132.1, 131.8, 130.9, 130.0, 129.5, 129.1, 128.8, 128.7, 128.0, 127.9, 127.7, 127.61, 127.56, 122.1, 121.1, 120.6, 103.0. UV-vis (CH_2Cl_2) λ [nm] ($\varepsilon/10^4$ [M^{-1} cm^{-1}]) = 292 (sh), 316 (2.18), 384 (sh), 438 (16.65), 496 (sh), 517 (1.28), 541(sh), 558 (0.92), 590 (sh), 619 (0.81), 640 (sh), 668 (1.29).

Crystallographic data

Ag**ICC**AuCl (CCDC 2394666): $C_{54}H_{45}Ag_{0.94}Au_{0.9}Cl_{2.84}N_5$, M_r = 1143.29, monoclinic, $P2_1/n$, a = 16.4860(2) Å, b = 9.15880(12) Å, c = 30.2897(4) Å, β = 92.7667(12)°, Z = 4, R = 0.0623 [$I \geqq 2\sigma(I)$], R_w = 0.1578 (all data), GOF = 1.037.

Au**ICC**AuCl$_3$ (CCDC 2394670): $C_{47}H_{30}Au_{1.9}Cl_{4.7}N_5$, M_r = 1205.61, triclinic, $P\bar{1}$, a = 9.41147(18) Å, b = 14.0313(3) Å, c = 16.8034(3) Å, α = 110.8961(17)°, β = 94.6483(15)°, γ = 100.4507(16)°, Z = 2, R = 0.0372 [$I \geqq 2\sigma(I)$], R_w = 0.0921 (all data), GOF = 1.059.

Au**NCP**AuCl$_3$ (CCDC 2394677): $C_{45.5}H_{30}Au_2Cl_6N_4$, M_r = 1239.37, monoclinic, $C2/c$, a = 19.8854(4) Å, b = 27.5952(6) Å, c = 8.02367(19) Å, β = 96.673(2)°, Z = 4, R = 0.0850 [$I \geqq 2\sigma(I)$], R_w = 0.2318 (all data), GOF = 1.119.

Ag**ICCI**rCp*Cl$_2$ (CCDC 2394665): $C_{71}H_{58}AgCl_2IrN_5$, M_r = 1352.19, triclinic, $P\bar{1}$, a = 12.6740(2) Å, b = 15.7863(2) Å, c = 16.6020(2) Å, α = 113.853(3)°, β = 99.635(2)°, γ = 101.492(2)°, Z = 2, R = 0.0230 [$I \geqq 2\sigma(I)$], R_w = 0.0593 (all data), GOF = 1.046.

ICC(BOPh)$_3$ (CCDC 2394671): $C_{130}H_{95}B_6N_{10}O_6Cl_4$, M_r = 2099.81, triclinic, $P\bar{1}$, a = 17.8280(3) Å, b = 17.84840(18) Å, c = 18.3446(2) Å, α = 73.5280(10)°, β = 71.5735(12)°, γ = 88.9914(11)°, Z = 2, R = 0.0499 [$I \geqq 2\sigma(I)$], R_w = 0.1376 (all data), GOF = 1.028.

Conflicts of interest

There are no conflicts to declare.

Data availability

The data supporting this article have been included as part of the supplementary information (SI). Supplementary information: additional spectroscopic, mass spectrometric, crystallographic, and electrochemical data. See DOI: https://doi.org/10.1039/d4dt03034f.

CCDC 2394665, 2394666, 2394670, 2394671 and 2394677 contain the supplementary crystallographic data for this paper.[83a–e]

Acknowledgements

This work was supported by the Polish National Science Center (2022/45/B/ST4/01229).

References

1 P. J. Chmielewski, L. Latos-Grażyński, K. Rachlewicz and T. Głowiak, *Angew. Chem., Int. Ed. Engl.*, 1994, **33**, 779–781.
2 H. Furuta, T. Asano and T. Ogawa, *J. Am. Chem. Soc.*, 1994, **116**, 767–768.
3 G. R. Geier III, D. M. Haynes and J. S. Lindsey, *Org. Lett.*, 1999, **1**, 1455–1458.
4 L. Latos-Grażyński and P. J. Chmielewski, *New J. Chem.*, 1997, **21**, 691–700.
5 M. Toganoh and H. Furuta, *Chem. Rev.*, 2022, **122**, 8313–8437.
6 M. J. Białek, K. Hurej, H. Furuta and L. Latos-Grażyński, *Chem. Soc. Rev.*, 2023, **52**, 2083–2144.
7 J. D. Harvey and C. J. Ziegler, *Coord. Chem. Rev.*, 2003, **247**, 1–19.
8 P. J. Chmielewski and L. Latos-Grażyński, *Coord. Chem. Rev.*, 2005, **249**, 2510–2533.
9 H. Furuta, H. Maeda and A. Osuka, *Chem. Commun.*, 2002, 1795–1804.
10 H. Furuta, T. Ishizuka, A. Osuka, Y. Uwatoko and Y. Ishikawa, *Angew. Chem., Int. Ed.*, 2001, **40**, 2323–2325.
11 A. Srinivasan, H. Furuta and A. Osuka, *Chem. Commun.*, 2001, 1666–1667.
12 H. Furuta, K. Youfu, H. Maeda and A. Osuka, *Angew. Chem., Int. Ed.*, 2003, **42**, 2186–2188.
13 H. Maeda, Y. Ishikawa, H. Matsueda, A. Osuka and H. Furuta, *J. Am. Chem. Soc.*, 2003, **125**, 11822–11823.
14 H. Furuta, T. Morimoto and A. Osuka, *Inorg. Chem.*, 2004, **43**, 1618–1624.
15 J.-C. Liu, T. Ishizuka, A. Osuka and H. Furuta, *Chem. Commun.*, 2004, 1908–1909.
16 M. Toganoh, T. Ishizuka and H. Furuta, *Chem. Commun.*, 2004, 2464–2465.
17 T. Morimoto, S. Taniguchi, A. Osuka and H. Furuta, *Eur. J. Org. Chem.*, 2005, 3887–3890.
18 M. Toganoh, J. Konagawa and H. Furuta, *Inorg. Chem.*, 2006, **45**, 3852–3854.
19 T. Niino, M. Toganoh, B. Andrioletti and H. Furuta, *Chem. Commun.*, 2006, 4335–4337.
20 M. Toganoh, T. Niino, H. Maeda, B. Andrioletti and H. Furuta, *Inorg. Chem.*, 2006, **45**, 10428–10430.
21 Y. Xie, T. Morimoto and H. Furuta, *Angew. Chem., Int. Ed.*, 2006, **45**, 6907–6910.
22 A. Srinivasan, M. Toganoh, T. Niino, A. Osuka and H. Furuta, *Inorg. Chem.*, 2008, **47**, 11305–11313.
23 M. Toganoh, T. Niino and H. Furuta, *Chem. Commun.*, 2008, 4070–4072.
24 D.-H. Won, M. Toganoh, H. Uno and H. Furuta, *Dalton Trans.*, 2009, 6151–6158.
25 T. Yamamoto, M. Toganoh and H. Furuta, *Dalton Trans.*, 2012, **41**, 9154–9157.
26 T. Yamamoto, M. Toganoh, S. Mori, H. Uno and H. Furuta, *Chem. Sci.*, 2012, **3**, 3241–3248.
27 T. Miyazaki, T. Yamamot, S. Mashita, Y. Deguchi, K. Fukuyama, M. Ishida, S. Mori and H. Furuta, *Eur. J. Inorg. Chem.*, 2018, 203–207.

28 T. Yamamoto, K. Mitsuno, S. Mori, S. Itoyama, Y. Shiota, K. Yoshizawa, M. Ishida and H. Furuta, *Chem. – Eur. J.*, 2018, **24**, 6742–6746.
29 T. Miyazaki, K. Fukuyama, S. Mashita, Y. Deguchi, T. Yamamot, M. Ishida, S. Mori and H. Furuta, *ChemPlusChem*, 2019, **84**, 603–607.
30 O. Iwanaga, K. Fukuyama, S. Mori, J. T. Song, T. Ishihara, T. Miyazaki, M. Ishida and H. Furuta, *RSC Adv.*, 2021, **11**, 24575–24579.
31 H. Furuta, T. Ogawa, Y. Uwatoko and K. Araki, *Inorg. Chem.*, 1999, **38**, 2676–2682.
32 H. Furuta, T. Ishizuka and A. Osuka, *J. Am. Chem. Soc.*, 2002, **124**, 5622–5623.
33 T. Morimoto, H. Uno and H. Furuta, *Angew. Chem., Int. Ed.*, 2007, **46**, 3672–3675.
34 J. D. Harvey and C. J. Ziegler, *Chem. Commun.*, 2002, 1942–1943.
35 C.-H. Hung, W.-C. Chen, G.-H. Lee and S.-M. Peng, *Chem. Commun.*, 2002, 1516–1517.
36 J. Wojaczyński, J. Maciołek and P. J. Chmielewski, *Chem. – Asian J.*, 2017, **12**, 643–647.
37 P. J. Chmielewski, *Angew. Chem., Int. Ed.*, 2005, **44**, 6417–6420.
38 H. Furuta, N. Kubo, H. Maeda, T. Ishizuka, A. Osuka, H. Nanami and T. Ogawa, *Inorg. Chem.*, 2000, **39**, 5424–5425.
39 P. J. Chmielewski and I. Schmidt, *Inorg. Chem.*, 2004, **43**, 1885–1894.
40 P. J. Chmielewski, B. Durlej, M. Siczek and L. Szterenberg, *Angew. Chem., Int. Ed.*, 2009, **48**, 8736–8739.
41 S. Koniarz, K. Szydełko, M. J. Białek, K. Hurej and P. J. Chmielewski, *Adv. Sci.*, 2024, **11**, 2306696/1–2306696/15.
42 J.-F. Longevial, S. Clément, J. A. Wytko, R. Ruppert, J. Weiss and S. Richeter, *Chem. – Eur. J.*, 2018, **24**, 15442–15460.
43 M. J. Crossley and J. A. McDonald, *J. Chem. Soc., Perkin Trans. 1*, 1999, 2429–2431.
44 J.-F. Lefebvre, D. Leclercq, J.-P. Gisselbrecht and S. Richeter, *Eur. J. Org. Chem.*, 2010, 1912–1920.
45 M. Lo, J.-F. Lefebvre, D. Leclerq, A. van der Lee and S. Richeter, *Org. Lett.*, 2011, **13**, 3110–3113.
46 J.-F. Lefebvre, M. Lo, D. Leclercq and S. Richeter, *Chem. Commun.*, 2011, **14**, 2976–2978.
47 J.-F. Lefebvre, M. Lo, J.-P. Gisselbrecht, O. Coulembier, S. Clément and S. Richeter, *Chem. – Eur. J.*, 2013, **19**, 15652–15660.
48 M. Abdelhameed, P.-L. Karsenti, A. Langlois, J.-F. Lefebvre, S. Richeter, R. Ruppert and P. D. Harvey, *Chem. – Eur. J.*, 2014, **20**, 12988–13001.
49 J.-F. Longevial, A. Langlois, A. Buisson, C. H. Devillers, S. Clément, A. van der Lee, P. D. Harvey and S. Richeter, *Organometallics*, 2016, **35**, 663–672.
50 J.-F. Lefebvre, J.-F. Longevial, K. Molvinger, S. Clément and S. Richeter, *C. R. Chim.*, 2016, **19**, 94–102.
51 Y. Kashiwagi, K. Ohkubo, J. A. McDonald, I. M. Blake, M. J. Crossley, Y. Araki, O. Ito, H. Imahor and S. Fukuzumi, *Org. Lett.*, 2003, **5**, 2719–2721.
52 G. B. Bodedla, H. Wang, S. Chang, S. Chen, T. Chen, J. Zhao, W.-K. Wong and X. Zhu, *ChemistrySelect*, 2018, **3**, 2558–2564.
53 S. Richeter, A. Hadj-Aissa, C. Taffin, A. van der Lee and D. Leclercq, *Chem. Commun.*, 2007, 2148–2150.
54 S. Shimizu, *Chem. Rev.*, 2017, **117**, 2730–2784.
55 Z. Li, L. Zhang, Q. Wu, H. Li, Z. Kang, C. Yu, E. Hao and L. Jiao, *J. Am. Chem. Soc.*, 2022, **144**, 6692–6697.
56 W. J. Belcher, M. Breede, P. J. Brothers and C. E. F. Rickard, *Angew. Chem., Int. Ed.*, 1998, **37**, 1112.
57 A. Weiss, H. Pritzkow, P. J. Brothers and W. Siebert, *Angew. Chem., Int. Ed.*, 2001, **40**, 4182–4184.
58 P. J. Brothers, *Inorg. Chem.*, 2011, **50**, 12374–12386.
59 A. M. Albrett, K. E. Thomas, S. Maslek, A. Młodzianowska, J. Conradie, C. M. Beavers, A. Ghosh and P. J. Brothers, *Inorg. Chem.*, 2014, **53**, 5486–5493.
60 W. J. Belcher, M. C. Hodgson, K. Sumida, A. Torvisco, K. Ruhlandt-Senge, D. C. Ware, P. D. W. Boyd and P. J. Brothers, *Dalton Trans.*, 2008, 1602–1614.
61 M. R. Rao and M. Ravikanth, *J. Org. Chem.*, 2011, **76**, 3582–3587.
62 T. K. Khan, M. Broering, S. Manthur and M. Ravikanth, *Coord. Chem. Rev.*, 2013, **257**, 2348–2387.
63 A. Młodzianowska, L. Latos-Grażyński, L. Szterenberg and M. Stępień, *Inorg. Chem.*, 2007, **46**, 6950–6957.
64 J. Beckmann, D. Dakternieks, A. Duthie, A. E. K. Lim and E. R. T. Tiekink, *J. Organomet. Chem.*, 2001, **633**, 149–156.
65 M. C. Haberecht, M. Bolte, M. Wagner and H.-W. Lerner, *J. Chem. Crystallogr.*, 2005, **35**, 657–665.
66 C. P. Brock, R. P. Minton and K. Niedenzu, *Acta Crystallogr., Sect. C: Cryst. Struct. Commun.*, 1987, **43**, 1775–1779.
67 J. Krumsieck and M. Bröring, *Chem. – Eur. J.*, 2021, **27**, 11580–11588.
68 W. Jentzen, X.-Z. Song and J. A. Shelnutt, *J. Phys. Chem. B*, 1997, **101**, 1684–1699.
69 W. Jentzen, J.-G. Ma and J. A. Shelnutt, *Biophys. J.*, 1998, **74**, 753–763.
70 M. A. Beckett, G. C. Strickland, K. S. Varma, D. E. Hibbs, M. B. Hursthouse and K. M. A. Malik, *J. Organomet. Chem.*, 1997, **535**, 33–41.
71 Q. G. Wu, G. Wu, L. Brancaleon and S. Wang, *Organometallics*, 1999, **18**, 2553–2556.
72 Y.-J. Wang, A.-Q. Jia, X.-S. Chen, H.-T. Shi and Q.-F. Zhang, *J. Chem. Crystallogr.*, 2015, **45**, 284–289.
73 M. A. Beckett, D. E. Hibbs, M. B. Hursthouse, P. Owen, K. M. A. Malik and K. S. Varma, *Main Group Chem.*, 1998, **2**, 251–258.
74 D. Ren, S. Koniarz, X. Li and P. J. Chmielewski, *Chem. Commun.*, 2020, **56**, 4856–4839.
75 H. Furuta, T. Ishizuka, A. Osuka and T. Ogawa, *J. Am. Chem. Soc.*, 1999, **121**, 2945–2946.
76 M. R. Churchill and S. A. Julis, *Inorg. Chem.*, 1977, **16**, 1488–1494.
77 K. M. Kadish, W. E, Z. Ou, J. Shao, P. J. Sintic, K. Ohkubo, S. Fukuzumi and M. J. Crossley, *Chem. Commun.*, 2002, 356–357.

78 E. Rabinovich, I. Goldberg and Z. Gross, *Chem. – Eur. J.*, 2011, **11**, 12294–12301.
79 G. M. Sheldrick, *Acta Crystallogr., Sect. A:Found. Adv.*, 2015, **71**, 3–8.
80 G. M. Sheldrick, *Acta Crystallogr., Sect. C: Struct. Chem.*, 2015, **71**, 3–8.
81 O. V. Dolomanov, L. J. Bourhis, R. J. Gildea, J. A. K. Howard and H. Puschmann, *J. Appl. Crystallogr.*, 2009, **42**, 339–341.
82 A. L. Spek, *Acta Crystallogr., Sect. C: Struct. Chem.*, 2015, **71**, 9–18.
83 (*a*) CCDC 2394665: Experimental Crystal Structure Determination, 2025, DOI: 10.5517/ccdc.csd.cc2lcv83; (*b*) CCDC 2394666: Experimental Crystal Structure Determination, 2025, DOI: 10.5517/ccdc.csd.cc2lcv94; (*c*) CCDC 2394670: Experimental Crystal Structure Determination, 2025, DOI: 10.5517/ccdc.csd.cc2lcvf8; (*d*) CCDC 2394671: Experimental Crystal Structure Determination, 2025, DOI: 10.5517/ccdc.csd.cc2lcvg9; (*e*) CCDC 2394677: Experimental Crystal Structure Determination, 2025, DOI: 10.5517/ccdc.csd.cc2lcvnh.